



Freestanding PTFE electrospun tubular membrane for reverse osmosis brine concentration by vacuum membrane distillation

Tao Zhou^{a,b}, Jingde Li^a, Xiaoming Guo^{a,b}, Yongyi Yao^{a,c,*}, Puxin Zhu^{a,*}, Ruili Xiang^d

^aTextile Institute, Sichuan University, Chengdu 610065, Sichuan, China, email: zhtgang@aliyun.com (T. Zhou), 2631430873@qq.com (J. Li), 593570521@qq.com (X. Guo), Tel. +86 28 85401819, email: yongyiyao@scu.edu.cn (Y. Yao), Tel. +86 28 85405437, email: zhupxscu@163.com (P. Zhu)

^bChengdu Biotop Pharma Tech. Co., Ltd. Chengdu 610041, Sichuan, China

^cNational Engineering Research Centre for Flue Gas Desulfurization Techniques, College of Architecture and Environment, Sichuan University, Chengdu 610065, Sichuan, China

^dAnalytical and Testing Center, Sichuan University, Chengdu 610064, Sichuan, China, email: xrlzxh8@sina.com (R. Xiang)

Received 15 January 2019; Accepted 5 June 2019

ABSTRACT

The desalination of highly concentrated brine wastewater is still a challenge in water treatment. In the present study, tubular polytetrafluoroethylene (PTFE) membranes were prepared by electrospinning and sintering method with the assistance of removable template. By increasing the membrane thickness, freestanding PTFE tubular membranes with sufficient strength and high liquid entry pressure value available in vacuum membrane distillation (VMD) were obtained. Their permeate flux and scaling behavior were further evaluated by VMD process for simulated reverse osmosis (RO) brine desalination. The results demonstrate that membrane scaling and permeate flux were highly related to the feed flowing conditions, especially in the saturation stage. The relationship of the salt crystallization mechanism, flowing disturbance conditions and VMD performance was further discussed. In proper flowing conditions, foulants mainly formed in the solution bulk and can be cleaned easily by the flushing of the feed flow. In four cycles of continuous concentration, the tubular membranes exhibit a steady performance of flux and rejection. These results shed light on the feasibility and prospect of the tubular electrospun membranes in high salinity brine desalination.

Keywords: Membrane distillation; Tubular membrane; PTFE; High salinity brine; Membrane scaling

1. Introduction

As an emerging desalination technology, membrane distillation (MD) technology has received a great deal of attention in recent years [1–4]. In the MD process, water vapors transport through a porous hydrophobic membrane under the vapor pressure difference between the feed and permeate side. According to the separation mechanism, MD can operate with reasonable fluxes under moderate temperature and pressure at high solution concentrations. Although MD technology has shown its promising application in the fields of seawater desalination [5,6], wastewater

treatment [7] and pure water production [8], the most particular application potential lies in the desalination of highly concentrated solutions, which are out of the scope of reverse osmosis (RO) [9].

Despite its many distinctive benefits, the MD process has yet to be widely implemented in industry. Membrane wetting danger is the major challenge for long-time operation in MD applications.

As a basic component in the MD system, the membrane has to be hydrophobic to ensure the retention of liquid, and only the vapor phase is allowed to pass through. Microfiltration membranes fabricated by hydrophobic materials, such as polypropylene (PP), polyvinylidene fluoride (PVDF) or polytetrafluoroethylene (PTFE), were widely tested in MD process [1]. However, even though hydrophobic mem-

*Corresponding author.

branes were used, pore wetting may still occur, because the membrane hydrophobicity was totally destroyed by unwanted deposits. Fouling is believed the major contribution to pore wetting [10].

Membrane fouling can be dependent on several factors, such as the degree of saturation, hydrodynamic conditions, solution compositions and membrane properties like roughness and morphology [10]. In general, membrane fouling can be reduced at high cross-flow velocity [11]. Enhancing the flowing dynamics can increase the flowing turbulence and reduce the polarization degree. Both are beneficial for mitigating fouling deposit. Good flowing distribution and adequate turbulence are highly decided by the membrane structure and the flow channel of the modules.

Regarding MD modules, flat sheet and hollow fiber are the two major module configurations in MD application [12]. Flat sheet membrane modules were widely employed in laboratory experiments for it is easy to construct and replace. However, the packing density of flat sheet modules were low, and good flow distribution was difficult to achieve in the frame channels [12]. Fluid dead zones caused by the vortex are not well resolved yet [13]. Hollow fiber-based modules can provide larger packing densities, which were attractive in commercial applications [4,14]. However, hollow fiber membranes have a high fouling tendency and are difficult to clean and maintain [12,15].

Tubular membrane modules were widely used in traditional membrane technologies, such as microfiltration (MF) and ultrafiltration (UF), but rarely proposed in the MD process for lower packing density [16]. Even though tubular membrane modules are more attractive than others because it is suitable for fluids of high velocity, which favorable for fouling reducing, easy cleaning and low tendency to polarization phenomena [4,12]. Comparing to flat sheet and hollow fiber modules, tubular membrane modules may be more suitable for highly concentrated solution treatment. On the other hand, unlike flat sheet membranes, tubular membranes are usually produced without support [1], which requires higher strength and stiffness. Thus, the few studies that test tubular membranes in the MD process mostly use membranes made of ceramic [17]. Polymeric tubular membranes have rarely been studied in MD, not to mention their fouling performance.

Recently, nanofiber membranes fabricated by electrospinning were tested in the MD process and show an attractive application performance [18,19]. Nanofiber membranes are believed to possess high porosity, high hydrophobicity, interconnected open pore structure and controllable membrane parameters, which are highly desirable for MD membranes. Tubular nanofiber membranes were widely proposed in tissue engineering as scaffolds [20,21] but that not been mentioned in MD applications to my knowledge. The mechanical strength of the electrospun membranes was the main concern, though less mechanical integrity was required in MD compared to other membrane separation processes. Nanofiber membranes can be enhanced by many methods, and increasing membrane thickness may be the most convenient and effective method. Khayet et al. [22,23] prepared self-sustained electrospun nanofibrous membranes with enhanced thickness and successfully applied them in direct contact membrane distillation (DCMD).

In a previous work [24], hydrophobic electrospun PTFE flat membranes with a water contact angle (WCA) above 150° and membrane porosity as high as 80% was fabricated by an electrospinning-sintering strategy. The membrane was further applied and evaluated in MD and displayed a stable salt rejection above 98.5% for inorganic salt solution desalination. In this paper, tubular PTFE nanofibrous membrane without support was fabricated with the assistance of a removable template. The mechanical properties and other membrane parameters of the prepared tubular membranes with various thicknesses were studied. The freestanding tubular membranes were further assembled in a tube-shell module for treating simulated RO brine by vacuum membrane distillation (VMD) process. The VMD performance and fouling conditions were also investigated.

2. Experimental

2.1. Materials

PTFE emulsion (FR301B, which contains 60 wt% of PTFE fine particles dispersing in water, PTFE particle size around 200 nm) was purchased from 3F Co. Ltd., China. PVA 1799 (with a polymerization degree of 1700 and a hydrolysis degree of 99.0%) was purchased from Sichuan Vinylol Factory, China.

The chemical agents used in this study, including sodium chloride (NaCl), potassium chloride (KCl), magnesium sulfate ($MgSO_4$), magnesium chloride ($MgCl_2$) and calcium sulfate ($CaSO_4$), were purchased from Chengdu Kelong Chemical Plant (Chengdu, China) and were all analytical reagents.

Deionized water and pure nitrogen were used in this study.

2.2. Feed water preparation

Simulated RO brine was used as the feed and was formulated according to the composition given by Ge et al. [25], which contains 32.61 g/L NaCl, 1.03 g/L KCl, 4.52 g/L $MgCl_2$, 2.91 g/L $MgSO_4$ and 1.80 g/L $CaSO_4$ in water.

2.3. Freestanding tubular membrane preparation

The process of preparing freestanding tubular membranes is illustrated in Fig. 1. The spinning solution was prepared by mixing 10 g of PVA aqueous solution with a concentration of 15% and 7.5 g of PTFE emulsion (60%). The mix solution was stirred for over 6 h at room temperature before usage.

PTFE/PVA composite fibrous membranes were then fabricated by electrospinning. 18 kV direct current voltage, generated by a DC high-voltage power supply (BGG, Beijing High-voltage Technology Co. Ltd., China), was applied on the spinneret, whose distance to the collector was around 20 cm. The collector, which also acts as a template, was around 8 mm in diameter and formed by a bundle of parallel iron wires. Electrospinning was processed at ambient temperature, and the relative humidity was around 40 to 60%.

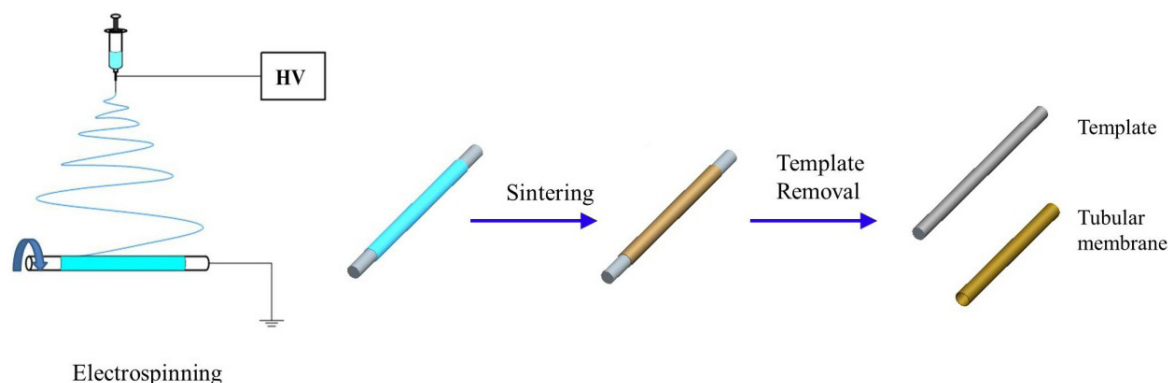


Fig. 1. Schematic illustration of the procedure for preparation of the tubular PTFE membrane.

By controlling the collection time, PTFE/PVA composite membranes with various thickness were obtained. The membrane together with the collector was vacuum dried at 80°C for 6 h and then sintered in an atmosphere tube furnace (JGL1200, Shanghai Jiugong Electric Co. LTD, China). The composite membrane was heated to 380°C in N₂ atmosphere and held for 30 min. Freestanding PTFE membrane was obtained by removing the iron wires after they cooled down.

2.4. Membrane characterization

The surface and cross-section of the membrane tubes were observed by scanning electron microscopy (SEM) (KYKY-2800, Shanghai).

The mechanical properties of the freestanding tubes were tested using an electronic fabric strength tester (YG065C, Laizhou Electron Instrument Co. Ltd., China). Tube samples with 60 mm in length were directly mounted on the sample clamps and were stretched at a strain rate of 100 mm/min. The respective thickness of each tube was measured by a pointer type pachymeter (CH-10-AT, Liuling Instrument Factory, Shanghai, China), whose measurement precision is 0.001 mm. Five specimens were tested for each sample to give the average values.

Water contact angle (WCA) measurements were performed using a DataPhysics OCAH200 goniometer equipped with a video capture device. Flat samples were cut off from the sintered tubular membranes and pasted on a flat glass slide. A deionized water droplet of approximately 4 μ L was deposited on the membrane surface. The corresponding images were captured to measure the WCA value. The WCA test was carried out at room temperature, and no less than five locations were tested for each sample.

Membrane pore size and distribution were characterized by a differential flow method [26] on a membrane pore size analyzer (3H-2000PB, Beijing Beiside Technology Apparatus Co. Ltd., China). Porofil, a low surface tension liquid (16 mN/m), was used as the wetting agent.

As tubular membranes, the liquid entry pressure (LEP) value was measured according to the method described in literature [27]. The pressure applied by compressed nitrogen was increased slowly and stepwise, and the pressure value at which the first drop of water appears on the outer surface was indicated as the LEP value of the given mem-

brane. The LEP values were also tested five times to give the average value for each membrane.

2.5. VMD experiment

To evaluate the VMD performance, the prepared tubular membranes whose inner diameter was 8 mm were further constructed into a tube-shell module. Since the membrane tube was self-sustained, the free ends of the tubular membrane with a glass tube collected as inner support were directly inserted through rubber plugs with a central hole. The rubber plugs were then tightly mounted on the glass shell. To precisely observe the flowing condition, one single membrane tube was studied in once testing. The tubular membranes tested in this study were around 200 mm in length. The prepared RO brine was circulated in the tube lumen of the membrane while vacuum applied on the shell side. The VMD set-up is illustrated in Fig. 2. In this study, the RO brine was circulated via a magnetic pump (MP-10R, Xishan Pumps Co. Shanghai, China), with a maximum hydraulic pressure of 115 kPa. The feed temperature and the pressure of the permeate side were fixed at 60°C and 5 kPa (–95 kPa shown on the vacuum pressure gauge), respectively.

For high salinity water treatment, simulated RO brine with an initial volume of 1 L was concentrated gradually until the residual solution was too little to circulate in the system. The different flowing conditions on the membrane performance were studied, and recirculation velocities of 0.17 m/s, 0.5 m/s and 1.0 m/s were performed for VMD testing. The permeate vapors were collected and measured by volume and conductivity (DDS-307A, INESA Scientific Instrument Co. Ltd., Shanghai, China) every 20 min.

After testing, the tubular membranes were carefully removed from the shell and were naturally dried to observe the deposited layers. Membrane cleaning was implemented by tap water flushing for 10 min.

A continuous VMD process was also carried out to investigate the online cleaning performance of the tubular module. The online cleaning was processed by pouring all the produced water back into the feed tank after every cycle of concentration. By that the feed brine was diluted to the initial concentration. The VMD testing was ongoing, and permeated vapors were collected and measured as before. Several concentration cycles were implemented contin-

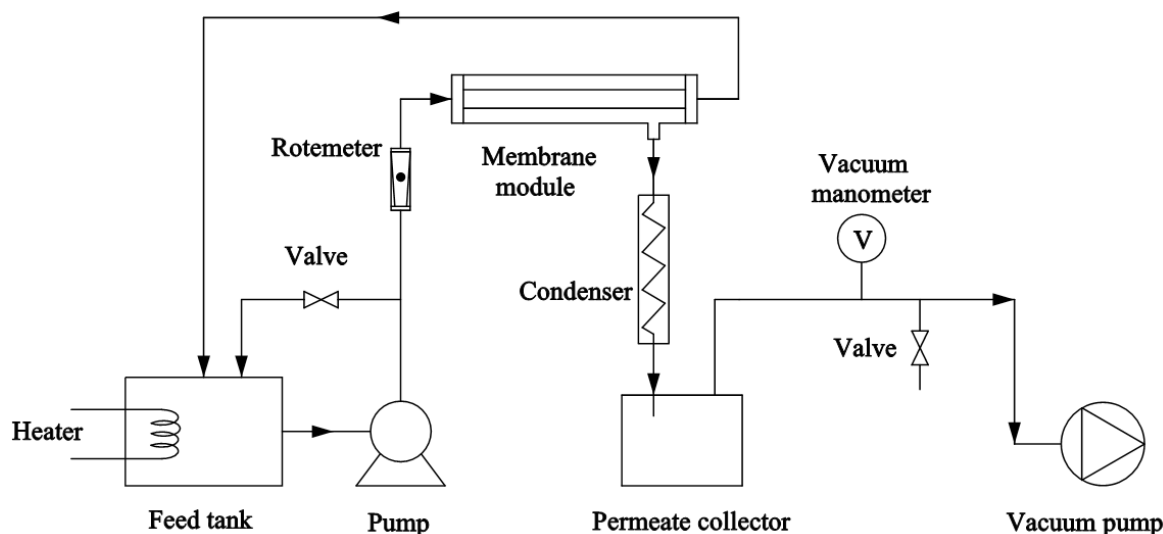


Fig. 2. Schematic diagram of the experimental set-up for VMD.

uously and the durability of the tubular membranes was evaluated by the flux recovery condition and the permeated water conductivity. No less than three samples were tested and cleaned in each mode.

3. Results and discussion

3.1. Freestanding tubular membrane and its morphology

Combined with the template approach, the PTFE nanofibrous tubes can be successfully fabricated by the electrospinning-sintering strategy. Fig. 3 shows the photo image of the tubular membranes, as well as SEM images of the tube outer and inner surfaces and the cross-section. We can see in Fig. 3 that, after template sintering, the fiber morphology of the inner surface obviously differed from the outer side. The outer surface of the tube was still constructed by nanofibers, which is similar to that proposed in previous literature [24]. The PTFE fibers of the inner side were no longer isolated from each other but formed interconnected fibrous networks with the intersecting points fused together. This is mainly attributed to the compaction between the shrinking fibers and the incompressible template. With the PVA component decomposing and the PTFE particles fusing in sintering, the centripetal shrinkage tightened the fiber layers and increasing fusion tendency of fibers in nearby layers. This also can be observed from the cross-section morphology of the tubular membranes (Fig. 3b). The tube wall was compact and symmetrical.

WCA images of the water drops deposited on the inner and outer surface of the membrane tube are also illustrated in Fig. 3, and the WCA values were $151 \pm 2^\circ$ and $156 \pm 2^\circ$, respectively. The hydrophobicity of the inner surface was slightly decreased by the compression in sintering. The surface roughness was believed to be decreased because of the fusion of the connection points of fibers [28]. However, since shrinkage is inevitable, and the inner surface is still hydrophobic though the WCA slightly decreased. The tubular membranes were also believed to be potential in MD application.

3.2. Mechanical properties of the freestanding tubular membranes

The fiber fusion in sintering was detrimental to hydrophobicity but was beneficial to the membrane strength. Typical stress-strain curves of the tubes before and after sintering are shown in Fig. 4a. In general, the precursor membranes before sintering were flexible and weak with the yield strength less than 1 MPa, while the elongation at break was up to 67%. After sintering, strong membranes are formed. The yield strength was above 4 Mpa, and the elongation at break was decreased to around 30%. Increasing membrane thickness will lead to a gradual enhancement of mechanical strength. For the sintered tubes, the yield strength was around 5.3 ± 1.2 MPa in a thickness range from 87 μm to 346 μm . For guarantee, reliable yield strength value of 4 MPa was further used to evaluate the tubular strength in case of damage deformation.

The variation of the mechanical properties of membranes before and after sintering could be explained by the evolution of the fiber structures during sintering process. The precursor nonwoven mat was constructed by randomly arranged fibers, which can easily adjust their orientation to the load and results in lower modulus of elasticity, higher value of elongation and a continuous increase of strength before breakage. The membrane strength was obviously enhanced in the sintering process because of the fusion of the nodes and the thickness compression.

In VMD application, the downstream vacuum pressure and the hydraulic pressure of the feed were the main loads applied on the membrane. As we know, the circular section pipeline is the best configuration for pressure vessels. The initial hoop stress at the tube wall due to internal fluid pressure can be conveniently estimated from the following equation [29]:

$$\sigma_t = \frac{PD}{2t} \quad (1)$$

where σ_t is the circumferential stress in Pa; P is the internal pressure in Pa; D is the diameter of the tube in meter and

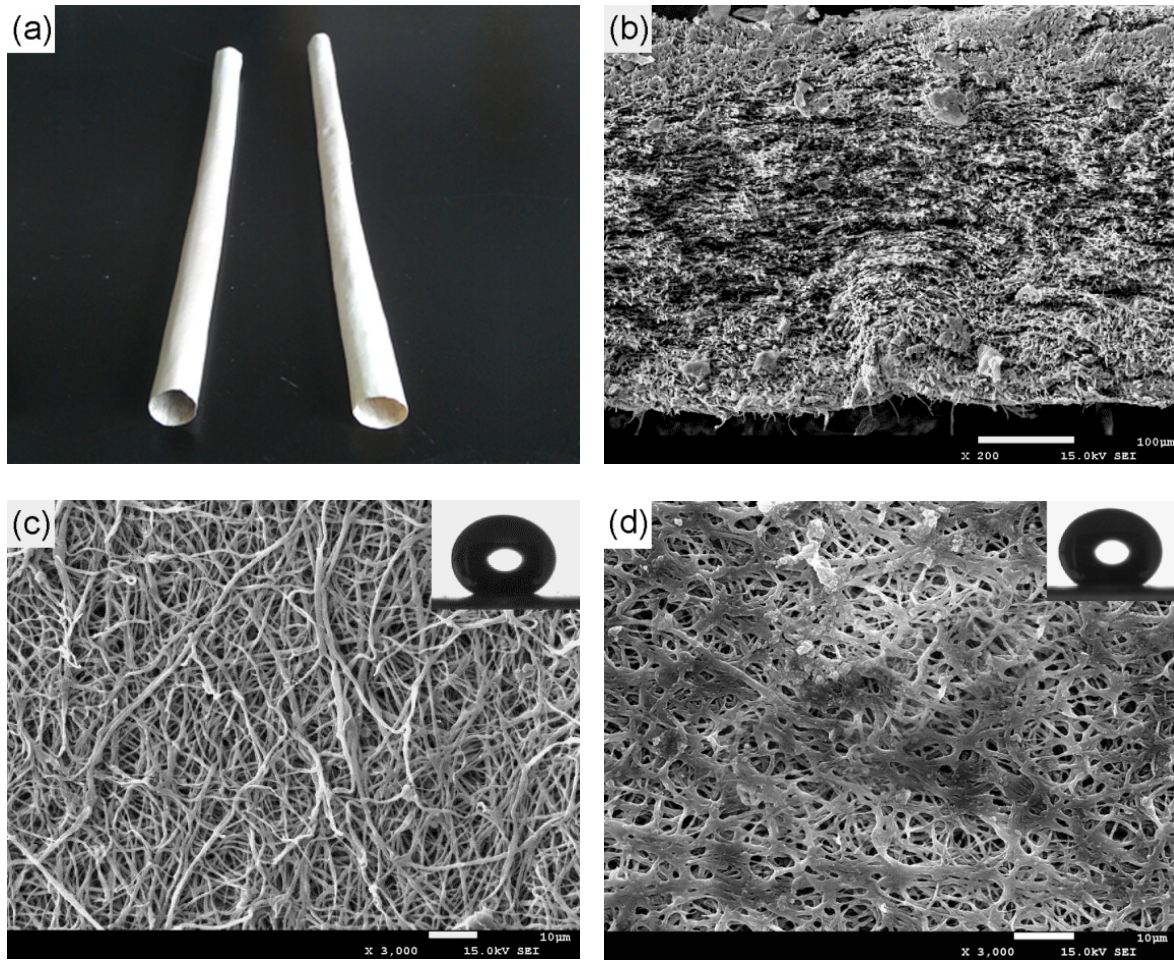


Fig. 3. Tubular membranes after sintering: (a) photo images; SEM images of (b) the cross-section, (c) outer surface and (d) inner surface, and the corresponding WCA images shown as insets.

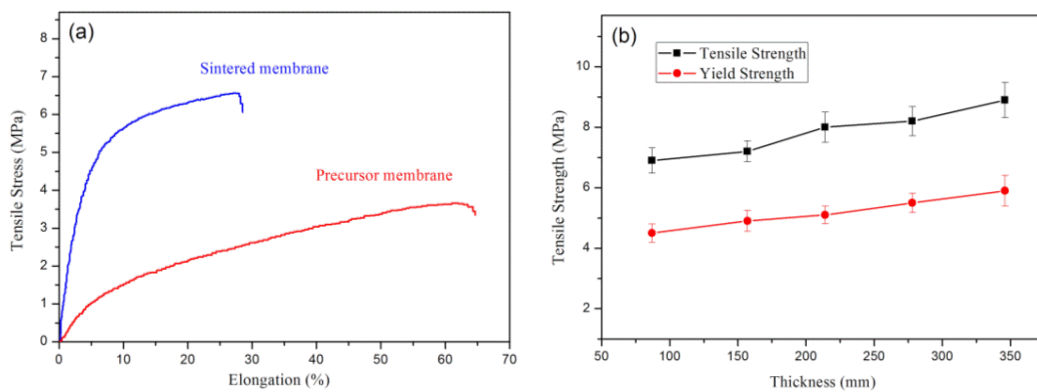


Fig. 4. (a) Typical stress–strain curves of the fibrous membranes before and after sintering. (b) Tensile strength and yield strength of the sintered tubular membranes with different thickness.

t is the thickness of the tube wall in meter. This formula is applicable when the wall thickness is much smaller compared to the outside diameter, $(D/t) \gg 1$.

In our study, the pressure applied on the tube wall was determined mainly by the pressure difference of the feed side (not exceeding the maximum hydraulic pressure of the

pump, 115 kPa) and the vacuum side (5 kPa in this study). So, the resultant load was less than 110 kPa. D is basically decided by the diameter of the template we used. From Eq. (1), we can figure out that thinner tubes with thicker wall will be more bearable for pressures. So hollow fiber membranes were usually self-sustained and were widely implemented

in pressure-driven filtrations. However, in the MD process, the narrow flow channels of hollow fibers lead to poor flowing dynamics and the resultant high degree of polarization phenomenon and fouling [12]. On the other hand, membrane thickness is an important character that affects MD performance. Thicker membranes were believed beneficial for reducing heat loss by conduction but also increase the mass transfer resistance. A membrane thickness of 10–60 μm is widely recommended by different authors for seawater desalination [2]. In high salinity applications, thicker isotropic hydrophobic membranes above 100 μm are required for improving the MD performance [2]. An optimal membrane thickness up to 700 μm was also proposed in some cases [2].

In our research, when the tube diameter was 8 mm, the applied pressure across the membrane wall was below 0.110 MPa, the circumferential stress should be less than 4 MPa, the yield strength of the membrane. The theoretical thickness available in VMD was calculated to be above 110 μm , without membrane yield deformation.

3.3. Effect of membrane thickness on characterizations

After sintering, enhanced tubular membranes with sufficient mechanical strength can be used as self-sustained. However, in VMD application, adequate LEP value was also required.

As an attractive approach for membrane fabrication, electrospinning technology was believed to be easy for tailoring membrane properties by adjusting electrospinning parameters. Fiber diameter and membrane thickness are highly correlated to the membrane pore size and distribution [30], which further affects the LEP value. Since the electrospinning and sintering parameters were fixed, the fiber diameter affection may be negligible. The pore size and LEP value were believed mainly determined by the membrane thickness.

By adjusting the collection time in the electrospinning process, composite membranes with a series of thicknesses were obtained. After sintering, the membrane pore size, LEP value and the corresponding thickness were measured and listed in Table 1.

We can see in Table 1 that membrane pore sizes and the corresponding LEP values were generally decreased with the membrane thickness increased. A considerable reduction of pore size was observed when the thickness increased from 87 μm to 214 μm . After that, it seemed difficult for

the pore size to further diminish, as the thickness largely increased. The effect of the membrane thickness seemed relatively limited. But when the membrane thickness increased, the pore size distribution became more centered, and the pore path was elongated, which made the membrane difficult to be wetted.

This phenomenon was also proven in the filtration application of electrospun membranes [30]. Since the pore sizes of electrospun membranes were actually the combination of the inter-fiber spaces of fiber layers, thicker membrane will lead to more intersected inter-fiber spaces and smaller pore size. As the electrospinning process continues, the newly deposited nanofibers can be seen as an added layer with larger inter-fiber spaces. Therefore, thicker fiber deposition will finally homogenize the pore size and reach a plateau value of pore size.

Although further increasing the membrane thickness was ineffective to reduce pore size, the newly increased layers can continuously narrow down the membrane pore size distribution, which results into higher LEP value of thicker membranes.

The water contact angles of the membranes were not significantly changed with the membrane thickness variation and were maintained in the range of 149.6–152.3°. This may be due to the similar surface that was constructed by nanofibers fabricated in the same conditions.

3.4. MD performance of tubular membranes for RO concentration

To evaluate the desalination performance, a set of tubular PTFE membranes with a thickness around $346 \pm 3 \mu\text{m}$ were prepared and used for further application. The RO brine was concentrated gradually to super-saturation in various feeding velocities, while the feed temperature and the downstream pressure was maintained steadily at 60°C and 5 kPa, respectively. Fig. 5 shows the permeate flux and conductivity variation in the concentration. The concentration factor (CF) was the ratio of the concentration in the concentrate to that in the initial feed solution.

In Fig. 5a, we can figure out that the permeate flux was improved with the feed rate increasing. The effect of the feed rate on the permeate flux has been widely studied. It is believed that a rise in the feed flowing velocity causes a rise in turbulence, a reduction of heat transfer resistance in the boundary layers, and a consequential rise in the mass transfer coefficient [12].

Though operation in different flowing velocities, all curves in Fig. 5a show a similar two-stages trend of the flux variation to the concentration increasing. In the primary stages, the flux reduction was near linear to the CF increasing, while in the second stage, when the concentration exceeded some critical CF points, a dramatic flux decline was observed.

Some researchers proposed a similar trend in treating high salinity solutions. The sharp reduction of the permeate flux in the second period was believed closely associated with salt crystallization [31]. The brine was supersaturated when exceeded a critical level, and the feed contents were quite different from that of the first stage.

In the first stage, before saturation, the flux reduction was mainly affected by the vapor pressure variation of the

Table 1

Membrane thickness (t), inner surface water contact angle, mean pore size (dm), and the liquid entry pressure (LEP) of the tubular PTFE membranes prepared with different thickness

Sample No.	Membrane thickness (μm)	Water contact angle ($^\circ$)	Mean pore size (μm)	Maximum pore size (μm)	LEP (kPa)
1	87	152.3	0.765	0.939	95
2	157	149.7	0.643	0.762	120
3	214	151.3	0.586	0.674	155
4	278	149.6	0.557	0.625	170
5	346	150.6	0.542	0.574	185

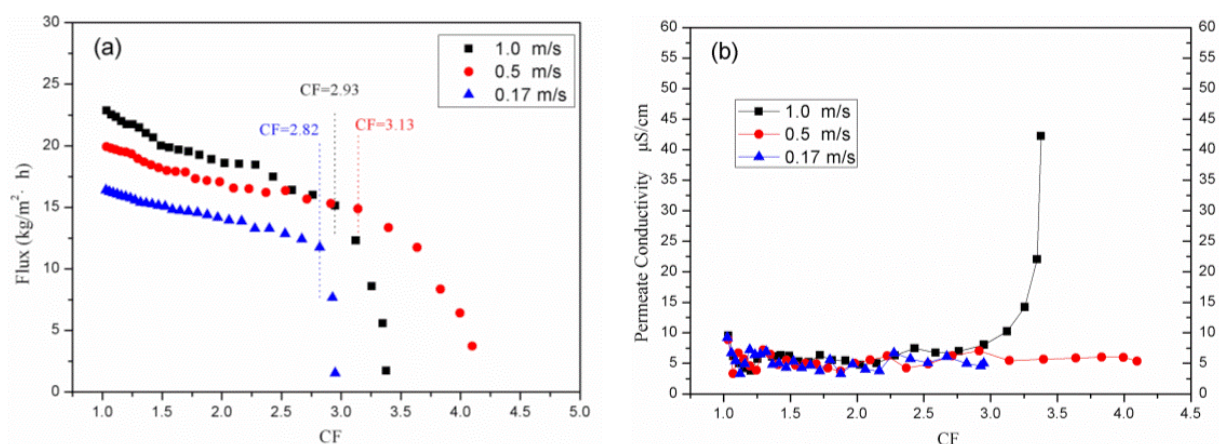


Fig. 5. Effect of the feed velocity on the permeate flux (a) and conductivity (b) at 60°C in 5 kPa VMD for RO brine treatment.

feed solution, which were proportional to the concentration, whose relationship was described by Raoult's Law. After that, crystals formed in the solution bulk or membrane surface resulted in an aggravated flux reduction. The crystal forming and depositing behavior were dramatically affected by the solution disturbance of the different operating conditions [32], which resulted in the different trends of flux variation in the second stage. Unlike in the first stage, the flux trend in the second stage was quite different when tested in different flowing conditions. Furthermore, the critical CF point was slightly affected by the operation conditions. The saturated CF in the feed velocities of 0.17 m/s, 0.5 m/s and 1.0 m/s shown in Fig. 5a was 2.89, 3.13 and 2.93, respectively. That can also be explained by the effect of agitation on the crystal formation rate and mechanism [32].

At lower circulating velocity of 0.17 m/s, once exceeds the critical concentration, the flux was dramatically decreased in a short period. It seemed that the membrane pores were rapidly blocked by the precipitates. While at higher velocity of 0.5 m/s or 1.0 m/s, the flux decreased much more gently. As we know, the brines flowing in tubular systems were equally distributed, and the shear rates introduced by high cross-flow velocity will effectively diminish the concentration polarization and promoted disturbance of the membrane surface regime. Both effects relieve the tendency for surface crystallization.

Furthermore, considering the distillate conductivity in Fig. 5b, when operated at high velocities of 1.0 m/s, membrane wetting occurred in the supersaturated stage. The permeate conductivity increased notably when the CF exceeded 3, while the conductivity of the permeated water was below 10 µS/cm and was maintained steadily in the first stage. This phenomenon may be attributed to the turbulent flow formed at high velocities. The turbulent flow enhanced the vertical hydrodynamic pressure on the membrane surface. The additional pressure may be negligible to the LEP value, but it may highly increase the collision probability between the crystals and the membrane inner wall, which may highly increase the tendency of surface crystallization and the risk of pore wetting.

To further investigate the crystal forming behavior, the deposited layer on the tube inner surface was observed after testing. The SEM images of the crystals formed in different

velocities are illustrated in Fig. 6. As we have discussed the effect of flowing condition on the crystallization rate, it also affects the crystal size and shape. At a slow velocity of 0.17 m/s, the crystals were well-shaped and show orthorhombic structure. The crystal size was large and completely covered the membrane surface.

The crystals formed at the velocity of 0.5 m/s were also well-shaped but much smaller in size. When operated at the flowing velocity of 1.0 m/s, the crystals were irregular in shape and non-uniform in size. We believed that the collisions and secondary nucleation dominated in the high shearing rate.

According to the above results, the flowing condition was critical in the high salinity brine treatment. Proper circulation velocity will not only effectively diminish the concentration and temperature polarization but will also flushing the particles away from the membrane surface to minimize fouling development.

3.4. Membrane cleaning

After testing at the flow velocity of 0.5 m/s, the membrane was further cleaned by off-line flushing. The membrane surface condition before and after cleaning was analyzed by SEM. The results are illustrated in Fig. 7.

We can see in Fig. 7 that after simple flushing, the accumulated crystals could be effectively removed, except for few residual salts formed in the drying process. We can presume that during the MD testing, foulants basically formed in the feed bulk instead of embedding in the membrane pores.

For further investigation, online cleaning was carried out by collected water poured back. The VMD performance of the continuous concentration is shown in Fig. 8. In four concentrating cycles, the VMD process displayed a similar two-stages trend in each treating cycle. The permeate flux decreased to a relatively low level when the brine was supersaturated at the end of each cycle, but followed by the distilled water poured in, the feed was diluted to under-saturated and the flux returned to a high level quite close to the initial value in a very short period. That may confirm that the crystals forming mechanical and weak adherence to the membrane surface. The shearing of the cross-flow veloc-

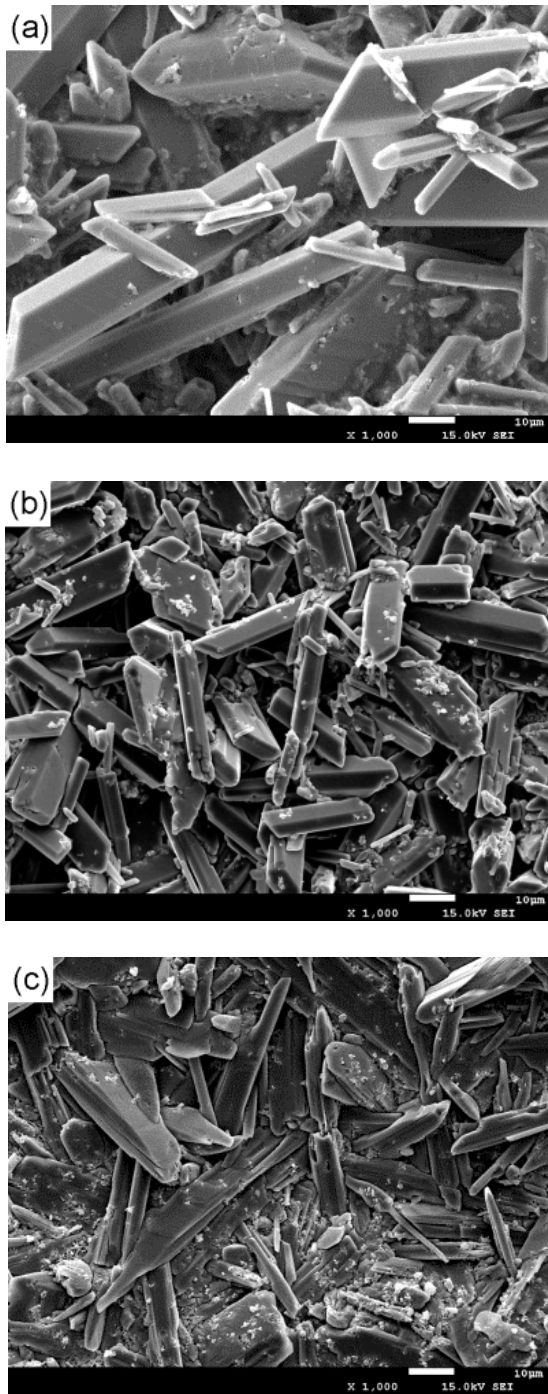


Fig. 6. SEM images of the crystals formed in the MD concentration at flow velocities of (a) 0.17 m/s, (b) 0.5 m/s and (c) 1.0 m/s.

ity in the tube lumen can easily peel the foulants away from the membrane surface.

This highly fouling resistance of the tubular membrane was mainly attributed to the increased lumen space, which available for higher flowing rate, comparing to the widely proposed hollow fibers. Several researches proposed that the slow internal flow in the fine hollow fibers often extreme concentration polariza-

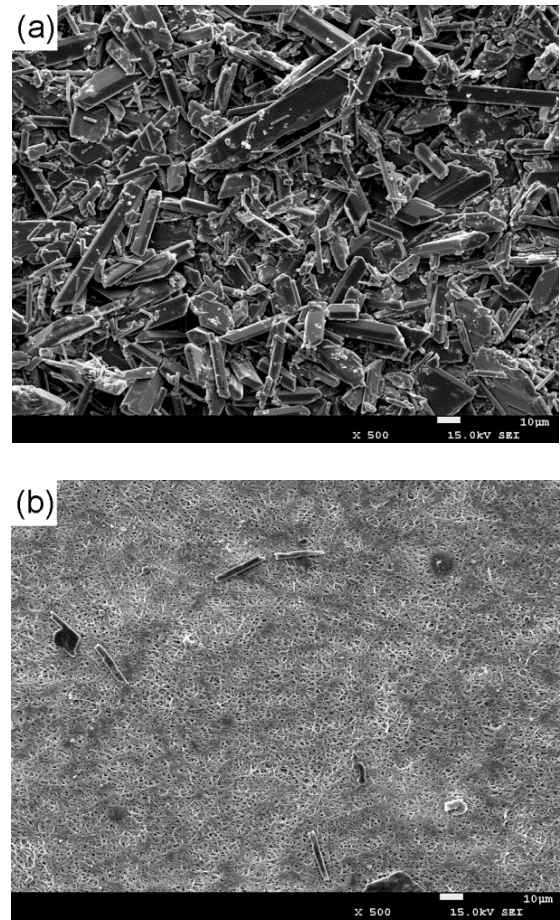


Fig. 7. SEM images of the used membrane (a) before and (b) after off-line cleaning.

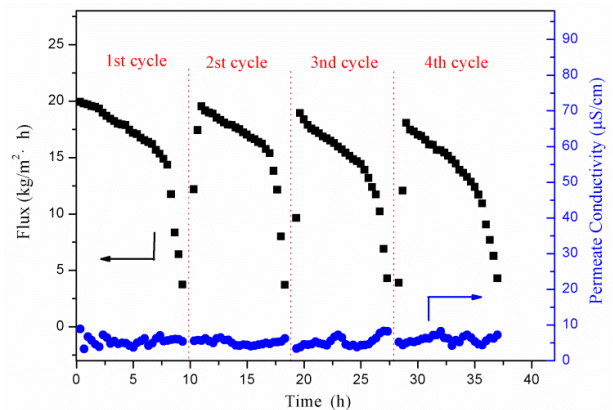


Fig. 8. Permeate flux and conductivity in continuous operation for RO brine concentration in the VMD process. The flow velocity, temperature and vacuum pressure were 0.5 m/s, 60°C and 5 kPa, receptivity.

tion and shown highly fouling potential even with bulk concentrations well below saturation [33]. The improved flowing dynamics in tubular membrane modules will effectively increase feed turbulence and resulted to a low

fouling potential. This further assure tubular membranes steadily applied in concentrating high salinity solutions without the traditional scaling mitigation method such as gas bubbling [31,34], membrane vibration [34] or ultrasound assistance [35,36], which need extra energy consumption.

In the continuous concentration process, the highest permeate flux slightly decreased from 19.92 kg/m²·h of the initial cycle to 18.06 kg/m²·h of the fourth cycle. The flux recovery was above 90%, compactable to those chemical cleaning methods [33], revealing the anti-fouling efficiency of tubular membranes.

During the continuous VMD process in 0.5 m/s flowing velocity, the permeate conductivity fluctuated in a small extent but was sustained to produce water with a conductivity lower than 10 µS/cm. Pore wetting was not observed. This also indicated the feasibility and durability of the tubular PTFE membranes applied in highly salinity brine treatment.

4. Conclusion

In summary, we found that freestanding PTFE electrospun tubular membranes can be prepared by an electrospinning and sintering method with the assistance of removable template. After sintering, the thickness compression due to fiber shrinkage helped enhancing the membrane strength and make the membranes self-sustainable. By increasing the membrane thickness, high LEP value membranes available in high salinity brine treatment by VMD were obtained.

Membranes with an 8 mm inner diameter and 346±3 µm thickness were successfully applied in simulated RO brine treatment by VMD.

The conclusions drawn in this work summarized as follows:

1. The freestanding PTFE electrospun tubular membranes exhibit a steady performance of permeate flux and rejection in the conditions in our study.
2. The permeate flux and fouling behavior of the tubular membranes shown a highly related to the operating feed rates. This phenomenon resulted from the effects of flow disturbance condition and crystallization mechanism in the tubular membranes.
3. The scaling layer on the membrane inner surface could be easily removed by flushing and the flux recovered above 90% after fourth desalination cycles, while the permeate conductivity maintained below 10 µS/cm during the cycles.

The present results suggest that the tubular membranes provide an ideal candidate membrane model for the desalination of highly concentrated brine.

Acknowledgements

This work is supported by National Natural Science Foundation of P.R.China (Grant No.50473050), and the Application and Basic Research Foundation of Sichuan Province (Grant No.2010JY0015).

References

- [1] M.S. Elbourawi, Z. Ding, R. Ma, M. Khayet, A framework for better understanding membrane distillation separation process, *J. Membr. Sci.*, 285 (2006) 4–29.
- [2] L. Eykens, K. De Sitter, C. Dotremont, L. Pinoy, B. Van der Bruggen, Membrane synthesis for membrane distillation: A review, *Sep. Purif. Technol.*, 182 (2017) 36–51.
- [3] H. Chamani, T. Matsuura, D. Rana, C.Q. Lan, Modeling of pore wetting in vacuum membrane distillation, *J. Membr. Sci.*, 572 (2019) 332–342.
- [4] K.W. Lawson, D.R. Lloyd, Membrane distillation, *J. Membr. Sci.*, 124 (1997) 1–25.
- [5] Y. Xu, B. Zhu, Y. Xu, Pilot test of vacuum membrane distillation for seawater desalination on a ship, *Desalination*, 189 (2006) 165–169.
- [6] J.-P. Mericq, S. Laborie, C. Cabassud, Vacuum membrane distillation of seawater reverse osmosis brines, *Water Res.*, 44 (2010) 5260–5273.
- [7] M. Gryta, M. Tomaszewska, K. Karakulski, Wastewater treatment by membrane distillation, *Desalination*, 198 (2006) 67–73.
- [8] C. Feng, K.C. Khulbe, T. Matsuura, R. Gopal, S. Kaur, S. Ramakrishna, M. Khayet, Production of drinking water from saline water by air-gap membrane distillation using polyvinylidene fluoride nanofiber membrane, *J. Membr. Sci.*, 311 (2008) 1–6.
- [9] J. Chaloupek, T. Lederer, Flux enhancement in membrane distillation using nanofiber membranes, *J. Nanomater.*, 2016 (2016) 1–7.
- [10] L.D. Tijing, C.W. Yun, J.S. Choi, S. Lee, S.H. Kim, H.K. Shon, Fouling and its control in membrane distillation—A review, *J. Membr. Sci.*, 475 (2015) 215–244.
- [11] P. Goh, W. Lau, M. Othman, A. Ismail, Membrane fouling in desalination and its mitigation strategies, *Desalination*, 425 (2018) 130–155.
- [12] L. Camacho, L. Dumée, J. Zhang, J.-d. Li, M. Duke, J. Gomez, S. Gray, Advances in membrane distillation for water desalination and purification applications, *Water*, 5 (2013) 94–196.
- [13] S. Soukane, M.W. Naceur, L. Francis, A. Alsaadi, N. Ghaffour, Effect of feed flow pattern on the distribution of permeate fluxes in desalination by direct contact membrane distillation, *Desalination*, 418 (2017) 43–59.
- [14] R. Baghel, S. Upadhyaya, K. Singh, S.P. Chaurasia, A.B. Gupta, R.K. Dohare, A review on membrane applications and transport mechanisms in vacuum membrane distillation, *Rev. Chem. Eng.*, 34 (2017) 73–106.
- [15] A. Alkudhiri, N.A. Darwish, N. Hilal, Membrane distillation: A comprehensive review, *Desalination*, 287 (2012) 2–18.
- [16] C.-K. Chiam, R. Sarbatly, Vacuum membrane distillation processes for aqueous solution treatment—A review, *Chem. Eng. Process.*, 74 (2013) 27–54.
- [17] S. Cerneaux, I. Strużyńska, W.M. Kujawski, M. Persin, A. Larbot, Comparison of various membrane distillation methods for desalination using hydrophobic ceramic membranes, *J. Membr. Sci.*, 337 (2009) 55–60.
- [18] L.D. Tijing, J. Choi, S. Lee, S. Kim, H.K. Shon, Recent progress of membrane distillation using electrospun nanofibrous membrane, *J. Membr. Sci.*, 453 (2014) 435–462.
- [19] C.-Y. Pan, G.-R. Xu, K. Xu, H.-L. Zhao, Y.-Q. Wu, H.-C. Su, J.-M. Xu, R. Das, Electrospun nanofibrous membranes in membrane distillation: Recent developments and future perspectives, *Sep. Purif. Technol.*, 221 (2019) 44–63.
- [20] D. Nisbet, J.S. Forsythe, W. Shen, D.I. Finkelstein, M.K. Horne, A review of the cellular response on electrospun nanofibers for tissue engineering, *J. Biomater. Appl.*, 24 (2009) 7–29.
- [21] W. He, Z. Ma, W.E. Teo, Y.X. Dong, P.A. Robless, T.C. Lim, S. Ramakrishna, Tubular nanofiber scaffolds for tissue engineered small-diameter vascular grafts, *J. Biomed. Mater. Res. A.*, 90A (2010) 205–216.
- [22] M. Essalhi, M. Khayet, Self-sustained webs of polyvinylidene fluoride electrospun nanofibers at different electrospinning times: 1. Desalination by direct contact membrane distillation, *J. Membr. Sci.*, 433 (2013) 167–179.

- [23] M. Essalhi, M. Khayet, Self-sustained webs of polyvinylidene fluoride electrospun nano-fibers: Effects of polymer concentration and desalination by direct contact membrane distillation, *J. Membr. Sci.*, 454 (2014) 133–143.
- [24] T. Zhou, Y. Yao, R. Xiang, Y. Wu, Formation and characterization of polytetrafluoroethylene nanofiber membranes for vacuum membrane distillation, *J. Membr. Sci.*, 453 (2014) 402–408.
- [25] J. Ge, Y. Peng, Z. Li, P. Chen, S. Wang, Membrane fouling and wetting in a DCMD process for RO brine concentration, *Desalination*, 344 (2014) 97–107.
- [26] T. Yunoki, K. Matsumoto, K. Nakamura, Pore size distribution measurements of nonwoven fibrous filter by differential flow method, *Membrane*, 29 (2004) 227–235.
- [27] J. Kujawa, W. Kujawski, S. Koter, K. Jarzynka, A. Rozicka, K. Bajda, S. Cerneaux, M. Persin, A. Larbot, Membrane distillation properties of TiO₂ ceramic membranes modified by perfluoroalkylsilanes, *Desal. Water Treat.*, 51 (2013) 1352–1361.
- [28] Y. Liao, R. Wang, M. Tian, C. Qiu, A.G. Fane, Fabrication of polyvinylidene fluoride (PVDF) nanofiber membranes by electro-spinning for direct contact membrane distillation, *J. Membr. Sci.*, 425–426 (2013) 30–39.
- [29] A. Ibrahim, Y. Ryu, M. Saidpour, Stress analysis of thin-walled pressure vessels, *Mod. Mech. Eng.*, 5 (2015) 1–9.
- [30] R. Wang, Y. Liu, B. Li, B.S. Hsiao, B. Chu, Electrospun nanofibrous membranes for high flux microfiltration, *J. Membr. Sci.*, 392–393 (2012) 167–174.
- [31] T. Zou, X. Dong, G. Kang, M. Zhou, M. Li, Y. Cao, Fouling behavior and scaling mitigation strategy of CaSO₄ in submerged vacuum membrane distillation, *Desalination*, 425 (2018) 86–93.
- [32] J. Garside, R.J. Davey, Invited review secondary contact nucleation: kinetics, growth and scale-up, *Chem. Eng. Commun.*, 4 (1980) 393–424.
- [33] D.M. Warsinger, J. Swaminathan, E. Guillen-Burrieza, H.A. Arfat, Scaling and fouling in membrane distillation for desalination applications: a review, *Desalination*, 356 (2015) 294–313.
- [34] H. Julian, S. Meng, H. Li, Y. Ye, V. Chen, Effect of operation parameters on the mass transfer and fouling in submerged vacuum membrane distillation crystallization (VMDC) for inland brine water treatment, *J. Membr. Sci.*, 520 (2016) 679–692.
- [35] D. Hou, L. Zhang, C. Zhao, H. Fan, J. Wang, H. Huang, Ultrasonic irradiation control of silica fouling during membrane distillation process, *Desalination*, 386 (2016) 48–57.
- [36] M. Qasim, N.N. Darwish, S. Mhiyo, N.A. Darwish, N. Hilal, The use of ultrasound to mitigate membrane fouling in desalination and water treatment, *Desalination*, 443 (2018) 143–164.